Ideal Thermal-Hydraulic Performance of Geothermal Power Systems Above 300 °C

Daniel W. Dichter

Quaise Energy

Keywords

High-temperature, flash, binary, dry steam, cycle, working fluid, exergy, efficiency, supercritical, superhot rock, SHR, utilization

ABSTRACT

Current geothermal power plants are characterized by geofluid production temperatures ranging from about 100-250 °C, with research underway to enable much higher temperatures. The range of 300 °C and above is considered herein, encompassing the region of "superhot rock", or SHR, defined as exceeding 375-400 °C. To quantify the potential of these systems, the exergetic power of a production well is assessed at its maximum flow capacity, as determined empirically by the onset of erosion. This indicates that at a given temperature, the power output potential is maximized where the geofluid production is most dense. Performance plateaus around the critical point, beyond which higher exergy is approximately offset by reduced mass flow rate. Three types of power cycles were considered: dry steam, flash, and binary, with each cycle corresponding to specific production conditions. Dry steam cycles were found to confer superior exergetic efficiency, but relatively low gross power output because of the characteristically low production density. Flash and binary cycles were found to be a significant improvement on an equal-temperature basis, with the lower exergetic efficiency compensated by a much higher mass flow rate. Single-, double-, and triple-stage cycles were considered for both flash and binary plants, and optimized for exergetic efficiency using gradient ascent algorithms. This yielded heuristics for the optimal design of both cycle types. For binary cycles specifically, pure water was selected as the working fluid of choice on the basis of its superior performance at high temperatures, as compared to the hydrocarbons characteristic of organic Rankine cycles (ORCs). The performances of flash and binary plants were found to be highly similar in the sense of thermal and exergetic efficiency. Diminishing returns were observed in both cycles, with a significant improvement from adding a second stage, and smaller, more localized improvements from a third. The choice between flash and binary may depend more on practical considerations such as geochemistry, reinjection requirements, and capital costs. Altogether, the plants considered herein have the potential to produce about 30 MWe gross per production well with an 8.5 inch minimum inner diameter, up to an order of magnitude more than is typical of current geothermal systems.

1. Introduction

A wide variety of methods have been used to generate electrical power from geothermal heat. Common to all such methods is the drilling of at least one well to produce hot geofluid from a subsurface reservoir, which may be either liquid, vapor, or a two-phase mixture. These wells typically have a minimum inner diameter of $D = 8.5$ inches (IFC/GeothermEx, 2013, p. 22; API 5CT, 2005, p. 185), and are drilled into hydrothermal reservoirs with depths of about 1-3 km (IFC/GeothermEx, 2013, p. 15). Recent global meta-analysis studied the distribution of gross capacity per production well, finding a mode of 3.0 ± 0.5 MWe, with more than 50% of wells between 4.0 ± 2.5 MWe (IFC/GeothermEx, 2013, p. 14).

Research is also underway to enable artificial reservoirs in subsurface rock with minimal pre-existing permeability or fluid content, referred to as enhanced or engineered geothermal systems, or EGS. For generality, this paper considers a geothermal reservoir of arbitrary origin, into which a single production and reinjection well are drilled. The reservoir is assumed to have sufficient pressure to achieve the maximum flow capacity of the production well, as described in the following section.

2. Production Hydraulics

The hydraulic aspect ratio of a production well, as its depth to diameter, is typically on the order of about 10,000, per the figures from the previous section. Drilling to greater depths and temperatures is expected to entail even higher aspect ratios. This extreme slenderness introduces a significant frictional pressure drop between the reservoir and surface. This can be seen from the Darcy-Weisbach equation (Çengel et al., 2012, p. 545):

$$\Delta P = \frac{1}{2} f \frac{L}{D} \rho v^2 \tag{1}$$

Where ΔP is the pressure drop, f is the friction factor, L is the pipe length, D is the pipe diameter, ρ is the fluid density, and v is the average, or superficial, flow velocity. The factor L/D expresses the pipe's aspect ratio, so $\Delta P \propto L/D$, and $\Delta P \to \infty$ as $L/D \to \infty$, all else equal.

Geofluid production can also be expressed in terms of internal flow:

$$\dot{m} = \rho A v \tag{2}$$

Where $\dot{m}$ is the mass flow rate, and A is the cross-sectional flow area. Substituting the expression for v in Eq. (2) into Eq. (1) equation and solving for $\dot{m}$ yields:

$$\dot{m} = \sqrt{\frac{\pi^2 \Delta P D^5 \rho}{8 f L}} \tag{3}$$

For a well with a certain D and L, subject to a certain ΔP between the reservoir and surface:

$$\dot{m} \propto \sqrt{\rho} \tag{4}$$

Neglecting the small dependence of f on the fluid conditions for the sake of approximation. Experiments suggest that the production of high-temperature geothermal systems may be limited

by erosion rather than pressure, even at conventional depths (Ingason et al., 2014). In other words, the production well may be sufficiently pressurized downhole to incur erosion in an open flow scenario. Thereby, safe operation requires controlling the wellhead pressure to limit the production mass flow rate.

The onset and acceptable rate limit of erosion in systems with internal flow are best determined by direct measurement under representative conditions. Without such information, a common empirical standard for two-phase flow states that:

$$v_e = \frac{c}{\sqrt{\rho}} \tag{5}$$

Where v_e is the erosional velocity, and c is an empirical constant, with suggested values of $c =$ 100-250 (ft/s)(lb/ft^3)$^{1/2}$ depending on the duty cycle, presence of solids, and the degree of corrosivity; $c = 100$ (ft/s)(lb/ft^3)$^{1/2}$ is used herein, with appropriate unit conversions (API, 1991, p. 23). The same empirical standard specifies a constant maximum flow velocity of 4.57 m/s [15 ft/sec] for liquid, which is essentially a special case of the two-phase correlation with $x = 0$, where x denotes quality, or dryness fraction. This arises because the density of saturated liquid water is approximately constant with respect to temperature. Vapor flows are more commonly pressure-limited rather than erosion-limited, but the two-phase correlation with $x = 1$ nonetheless provides guidance as to the maximum vapor flow conditions. Supercritical flows are likewise assumed to be limited by the same empirical proportionality, noting that material properties at these higher temperatures require special consideration.

Substituting the expression for v_e in Eq. (5) into Eq. (2) such that $v = v_e$ yields an expression for the maximum mass flow rate of an erosion-limited internal flow:

$$\dot{m} = c\, A \sqrt{\rho} = \frac{\pi}{4}\, c\, D^2 \sqrt{\rho} \tag{6}$$

With respect to fluid properties, this is a restatement of the Darcy-Weisbach equation; namely:

$$\dot{m} \propto \sqrt{\rho} \tag{7}$$

Supposing geofluid production is erosion-limited, with a production pressure no higher than 300 bar per the approximate limitations of current boilers (Çengel et al., 2012, p. 387), the maximum mass flow rate is shown in Figure 1 below.

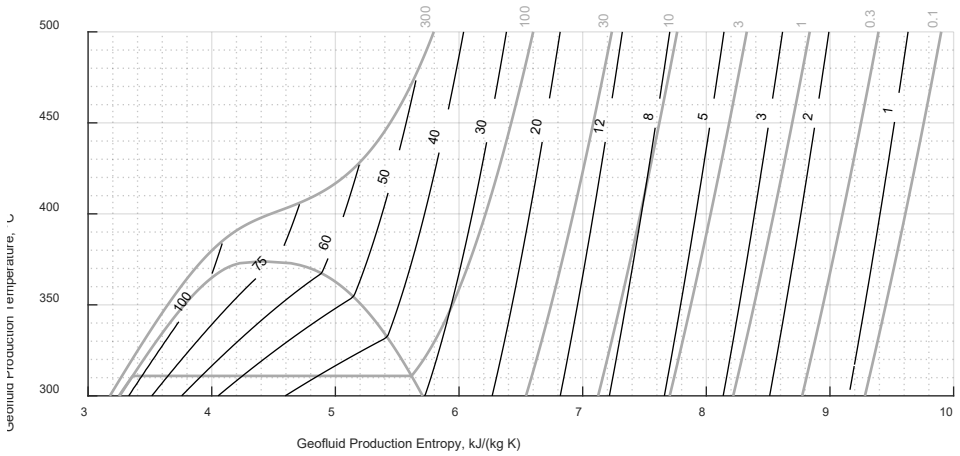

Figure 1: Contours of constant mass flow rate $\dot{m}$ in kg/s (black) for an erosion-limited well with D = 8.5". Overlaid in gray are the phase boundary of water, and a set of isobars labeled in units of bar.

This shows that in the subcritical region, $\dot{m}$ is substantially higher in the liquid phase than the vapor phase, with more than a 3:1 ratio at 300 °C. This disparity decreases to zero as $T \rightarrow T_{crit}$, i.e. as T approaches the critical temperature. In the supercritical region where $T > T_{crit}$, $\dot{m}$ decreases with T on an isobaric basis, because isobaric heat additions strictly decrease density.

3. Exergetic Power

Exergy expresses the maximum amount of work that can be obtained from a substance as it is brought into equilibrium with its surroundings, and can be used to calculate the potential power output of a geofluid flow. Its standard definition in the field of geothermal power is:

$$e = (h - h_o) - T_o\,(s - s_o) \tag{8}$$

Where e is exergy, h is enthalpy, and s is entropy, all of which are specific, or per unit mass; the subscript o refers to the dead state, and T_o is specified in consistent absolute units, e.g. Kelvin (DiPippo, 2016, pp. 295-296). The dead state is commonly taken as saturated liquid, and can thereby be defined by a temperature. The value of T_o = 50 °C [323.2 K] is used herein, assuming that heat rejection requires a temperature difference of at least ΔT = 10 °C with respect to a maximum ambient temperature of 40 °C [104 °F] (DiPippo, 2016, p. 128). This represents the anticipated condenser temperature, below which no work can be obtained. Exergetic power, denoted $\dot{E}$, is then given by:

$$\dot{E} = e\,\dot{m} \tag{9}$$

This quantity expresses the maximum power output, e.g. in MWe gross, associated with a geofluid flow, and is shown in Figure 2 below.

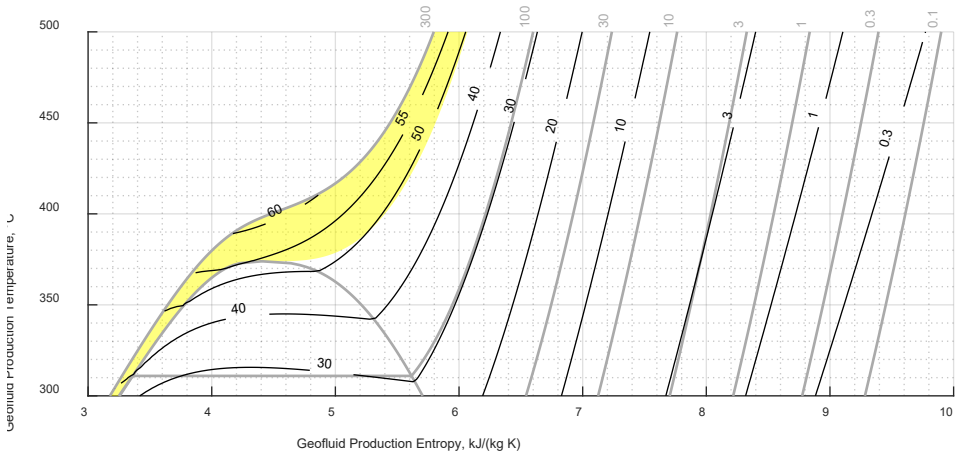

Figure 2: Contours of constant exergetic power $\dot{E}$ in MWe (black) for an erosion-limited well with D = 8.5". Overlaid in gray are the phase boundary of water, and a set of isobars labeled in units of bar. Highlighted in yellow is the region where exergetic power $\dot{E}$ is maximized for a certain production temperature, bounded by $x = 0$ where $T < T_{crit}$, $P = P_{crit}$ where $T > T_{crit}$, and P = 300 bar.

Similar to the earlier plot of $\dot{m}$, this shows in the subcritical region that liquid conveys substantially more exergetic power than vapor. This ratio is about 4:3 at 300 °C, again decreasing to zero at the critical point. In the dry steam and supercritical regions, $\dot{E}$ is approximately constant with respect to T on an isobaric basis, indicating that increases in h and e are offset by decreases in ρ and $\dot{m}$. For a given production temperature, exergetic power $\dot{E}$ is maximized where the production pressure is itself maximized, corresponding to a region spanning both compressed liquid and supercritical fluid. This region is characterized by production pressures of $P >$ 85.9 bar in the subcritical region, and $P >$ 220.6 bar in the supercritical region, per the saturation pressures at 300 °C and the critical pressure, respectively.

Typically, geothermal power plants attain around 25-65% of exergetic power, depending on the type and sophistication of the thermodynamic cycle, which itself is influenced by the geofluid production conditions (DiPippo, 2016, p. 243). This fraction is referred to as exergetic efficiency, or utilization, and is denoted by η_{II}, with the subscript II referring to the Second Law of Thermodynamics on which exergy is based. This is given by:

$$\eta_{II} = \frac{\dot{Q}}{\dot{E}} \tag{10}$$

Where $\dot{Q}$ denotes the gross power output of the plant, itself given by:

$$\dot{Q} = \dot{m}\, w_{net} = \dot{m}\, (q_{in} - q_{out}) \tag{11}$$

Where w_{net} is the net work, q_{in} is the heat input, and q_{out} is the heat rejection. The expression for η_{II} can be simplified to:

$$\eta_{II} = \frac{w_{net}}{e} \tag{12}$$

Note that this neglects parasitic loads from fans, pumps, lights, etc. for simplicity and generality, which are briefly discussed later. This is not to be confused with the more common thermal (or First Law) efficiency η_I, given by:

$$\eta_I = \frac{w_{net}}{q_{in}} = 1 - \frac{q_{out}}{q_{in}} \tag{13}$$

The remainder of this paper seeks to quantify how the value of η_{II} depends on the geofluid production conditions, the type of power cycle, and the cycle's relative sophistication. Thereby, the competing tradeoffs between $\dot{m}$, e, and η_{II} can be balanced, so that local and global optima for $\dot{Q}$ can be found.

4. Cycle Regions

The simplest method of generating power from a geofluid flow is a dry steam power cycle. This entails producing geofluid as a saturated or superheated vapor, then expanding it in a steam turbine, producing work. The basic constraint of this cycle is that the turbine must not have excessive condensation; herein, it is assumed that $x \geq 85\%$ throughout the turbine, based on typical manufacturers' specifications. These cycles also lack reheating, a common feature of non-geothermal plants, because it is not practical to re-flow the geofluid through the reservoir at an intermediate pressure once produced, unlike e.g. with fossil-fired boilers.

After the steam is expanded in the turbine, the residual waste heat is then rejected to ambient conditions by a condenser, as in a Rankine cycle. This imposes an additional constraint that the turbine outlet pressure cannot be lower than about 0.12 bar, the saturation pressure corresponding to 50 °C, the nominal heat rejection temperature.

The performance of the turbine can be described primarily by its dry isentropic, or nominal, efficiency η_{td}, which expresses the ratio of the actual enthalpy change of the steam between the inlet and the outlet, to this same quantity under isentropic conditions without the presence of condensation (Çengel et al., 2012, p. 383). This is taken as 85% herein (DiPippo, 2016, p. 122). Secondarily, the Baumann rule states that turbine efficiency decreases about 1% for each 1% of condensation, in the sense of quality x, according to empirical observations (DiPippo, 2016, p. 122).

Using numerical methods, a turbine process curve can be calculated, representing the set of inlet conditions corresponding to the turbine and condenser specifications described earlier. This curve intersects $x = 1$ at approximately $T = 190$ °C, the approximate maximum saturated vapor temperature for a dry steam power cycle, closely matching actual plants of this type (Calpine Corporation, 2023).

The region in T-s, or temperature-entropy, coordinates to the right of this curve represents the set of acceptable turbine inlet conditions, all of which is superheated vapor. To the left of this curve are regions of superheated vapor (generally, at lower enthalpy), supercritical fluid, saturated vapor, saturated liquid, compressed liquid, and two-phase mixtures. These two regions are denoted as A and B, as shown in Figure 3 below. The boundary between these regions can be approximated by the isentropic curve of $s = 6.236$ kJ/(kg K) over 300-500 °C.

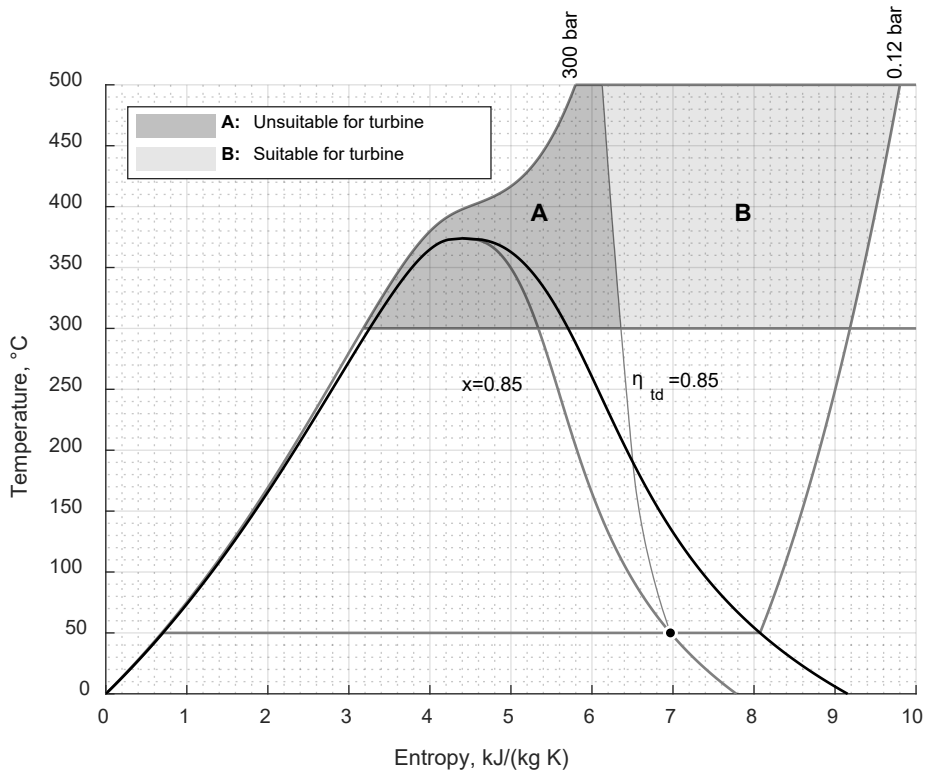

Figure 3: A T-s diagram of water divided into two regions, A and B, based on suitability for supplying typical non-reheat steam turbines.

As will be shown, η_{II} is maximized in dry steam power cycles, because no processing of the geofluid is required to yield vapor suitable for a turbine, which is inherently destructive of exergy. Therefore, this is considered as the most suitable cycle in Region B. In Region A, this type of cycle is not possible, so flash and binary cycles are considered instead. The following three sections describe each of these power cycles in greater detail.

5. Dry Steam Cycles

A dry steam power cycle is essentially a non-reheat Rankine cycle (Çengel et al., 2012, pp. 379-393). The cycle is assumed to be closed by an isobaric heat addition (2-3) for the sake of analysis, so that q_{in}, q_{out}, and w_{net} can be determined. Otherwise, this entails an isobaric rejection of residual heat in a condenser, and an isentropic pumping process. A plant schematic and representative T-s diagram are shown in Figures 4 and 5 below.

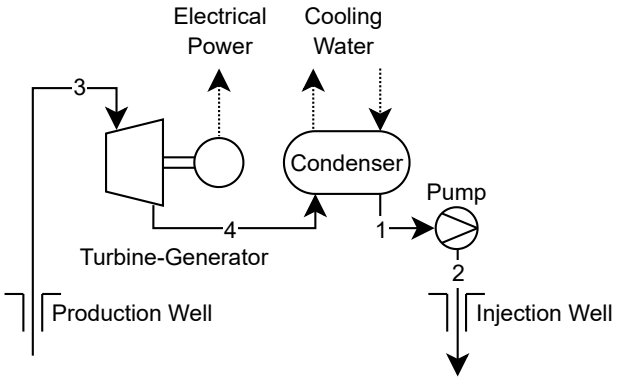

Figure 4: Schematic of a dry steam plant, not to scale.

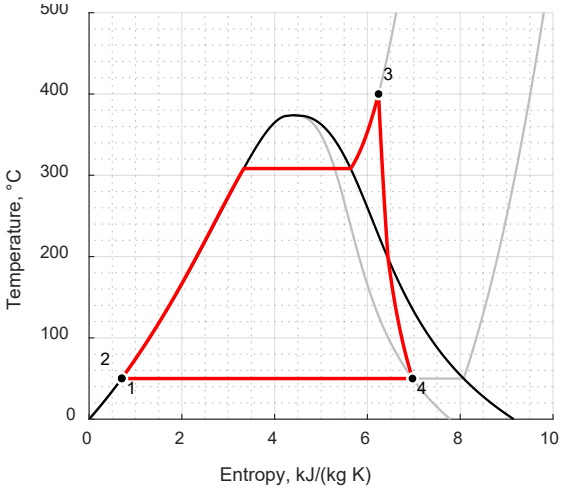

Dry Steam (Non-Reheat Rankine) Cycle

fluid	water	
q_in	2886.0	kJ/kg
q_out	2025.5	kJ/kg
w_net	860.5	kJ/kg
η_I	0.298	~
η_II	0.778	~
x_min	0.850	~

	T	P	h	s	x
1	50.0	0.12	209.6	0.70	0.000
2	50.3	96.45	219.3	0.70	NaN
3	400.0	96.45	3105.3	6.24	NaN
4	50.0	0.12	2235.0	6.97	0.850

Figure 5: T-s diagram of a representative dry steam power cycle with $T = 400$ °C at the turbine inlet, and $x = 0.85$ at the turbine outlet.

Evaluating all cycles in the region of interest, Region B, together with the hydraulic constraints for $\dot{m}$ described earlier, yields the plot shown in Figure 6 below.

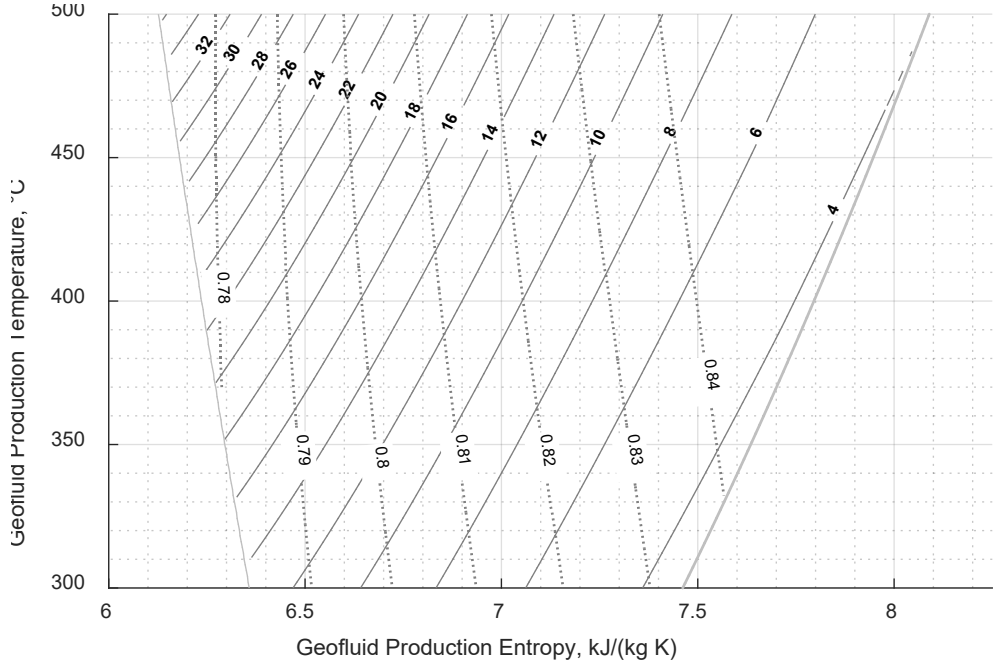

Figure 6: Gross power output in MWe (solid) and exergetic efficiency (dotted) for ideal dry steam cycles. The region of interest is bounded by $\eta_{td} = 0.85$, and $P = 5$ bar.

Although this region shows relatively high exergetic efficiency, this quantity is maximized where ρ and $\dot{m}$ are minimized. The maximum power output $\dot{Q}$ of about 32-34 MWe occurs around 475-500 °C and 150-200 bar, i.e. where the geofluid density ρ is maximized. Per Figure 2, it is anticipated that production in Region A should attain comparable power outputs at significantly lower temperatures, even accounting for the higher exergy in Region B. Thereby, wells producing in Region A could be significantly shallower than in Region B for the same $\dot{Q}$, entailing less capital cost associated with drilling. A further difficulty of producing steam at these extreme conditions is its relatively high compressibility, which typically results in a large frictional pressure drop ΔP between the reservoir and surface. Thereby, sufficiently deep reservoirs may not practically be able to produce at these conditions, because of the characteristic slenderness of the production well.

6. Flash Cycles

Flash cycles work by expanding a liquid-dominated geofluid, separating the resulting saturated vapor, and supplying it to a steam turbine. This is possible because isenthalpic expansion of saturated liquid or two-phase mixtures strictly increases quality x, though it also decreases exergy e. More sophisticated arrangements introduce a second, or less commonly, a third, flash-separation process, yielding higher exergetic efficiency.

Ideal flash cycles are characterized by isenthalpic flash processes, and isobaric separation processes (DiPippo, 2016, pp. 107-163). The separators are assumed to yield separate streams of saturated liquid and saturated vapor. Mixing of fluid streams is assumed to be isobaric, and is governed by conservation of mass and energy. Likewise, the condenser is assumed to be isobaric, and to yield saturated liquid. After leaving the condenser, the geofluid is pumped to the pressure of the final separator and mixed with the residual un-flashed liquid. This yields the final outlet conditions of moderately compressed liquid at an intermediate temperature between that of the condenser and the final separator. A schematic is shown in Figure 7 below.

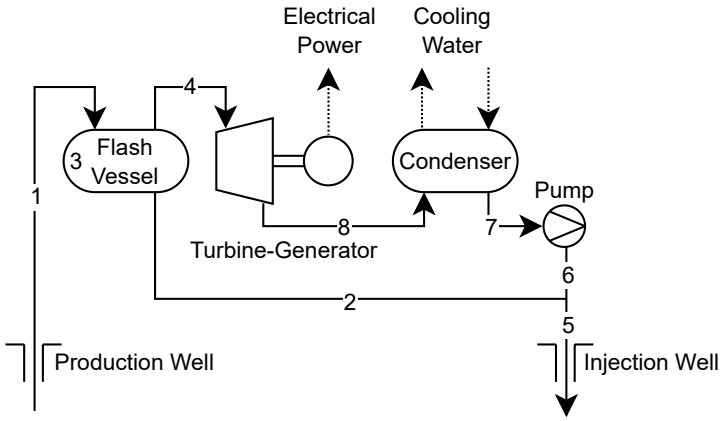

Figure 7: Schematic of a single-flash plant, not to scale.

Conventional geofluid production conditions for flash plants range from about 100-200 °C and $0.1 < x < 0.9$ (Zarrouk and Moon, 2014, pp. 147-148). Because this is generally less than the maximum saturated vapor temperature at the turbine inlet of 190 °C, as derived earlier, geofluid is conventionally separated rather than flashed once produced (DiPippo, 2016, p. 115). However, at the higher temperatures considered herein, the produced geofluid must instead be flashed before it can be separated, to achieve sufficient turbine dryness.

Only a subset of Region A is suitable for flash cycles. Of particular significance is the maximum enthalpy of saturated vapor: where $h >$ 2,800 kJ/kg, isenthalpic expansion generally yields superheated vapor, not a two-phase mixture, as shown in Figure 8 below.

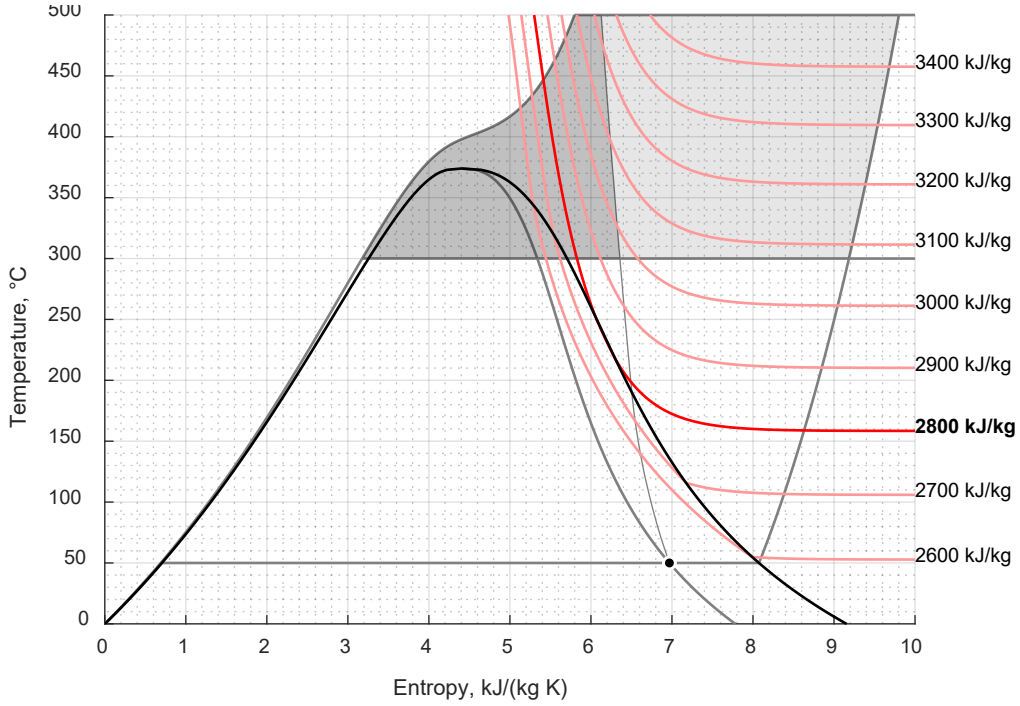

Figure 8: Cycle regions from Figure 3 overlaid with isenthalpic contours in the superheated vapor region. Highlighted is h = 2,800 kJ/kg, the approximate maximum enthalpy of saturated vapor, i.e. x = 1.

In the subset of Region A where $h >$ 2,800 kJ/kg, unconventional cycles could nonetheless be developed, for example by expanding the produced geofluid until intersecting the turbine process curve with $\eta_{td} = 0.85$, or by expanding the geofluid in the turbine and separating out the liquid condensate at least once to maintain sufficient dryness, incorporating elements of both dry steam and flash cycles. However, comparing Figures 2 and 8 indicates that the exergetic power $\dot{E}$ in this subset of Region A is relatively low, as compared to where $h <$ 2,800 kJ/kg, on an equal-temperature basis. For this reason, only the subset of Region A where $h <$ 2,800 kJ/kg is considered further in this section.

Given the turbine and condenser specifications described earlier, the main parameters required to define the flash cycle are the quantity of flashes, and the associated separator temperature(s). Conventionally, the optimal separator temperature(s) are well-approximated by the "equal-temperature-split" rule, or ETS, which states that the temperature differences between the inlet, any/all separator(s), and the condenser, are all mutually equal, regardless of the number of flashes (DiPippo, 2016, p. 132).

However, ETS has only limited applicability to high-temperature flash cycles, for two reasons. First, ETS assumes that saturated liquid water has a constant specific heat capacity C_p with respect to temperature. This is accurate to within ±3.6% over 0-200 °C, i.e. over the conventional temperature range for flash plants, but rapidly deteriorates at higher temperatures approaching the critical point, as shown in Figure 9 below. Specific heat at the critical point is effectively undefined, in the sense that $C_p \to \infty$, and $\partial T/\partial h \to 0$, as $T \to T_{crit}$, i.e. heat addition produces no

sensible temperature change, as with vaporization or condensation. Second, it can be shown that ETS generally yields deficient turbine outlet qualities for inlet conditions in Region A.

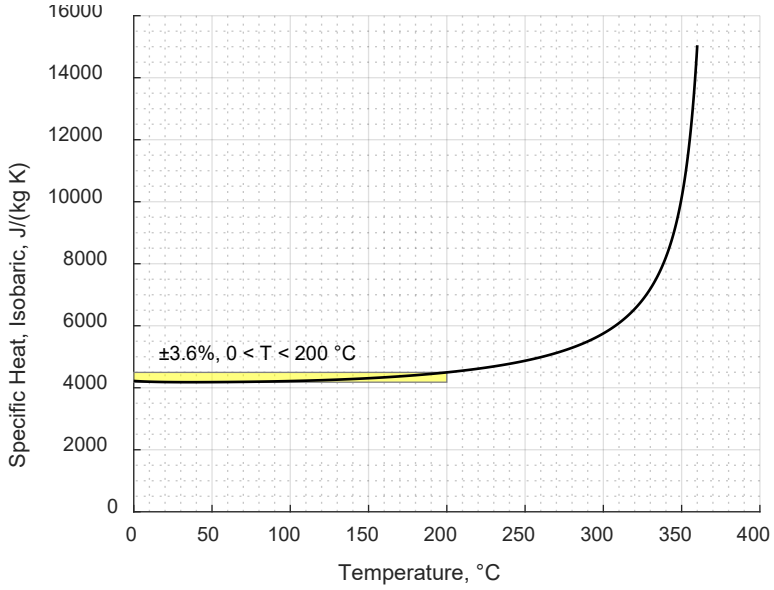

Figure 9: Specific heat capacity of saturated liquid water, showing that relative constancy (highlighted, yellow) breaks down above about 200 °C, as $T \rightarrow T_{crit}$.

Instead, a gradient ascent algorithm is used to determine the optimal separator temperature(s), in the sense of η_{II}, or equivalently w_{net}, with a step size of 1 °C. Although this method is not guaranteed to find global optima because of possible local maxima in w_{net}, its results compared favorably against exhaustive evaluation for select cases. Optimization is constrained such that no separator operates under vacuum, which is generally considered impractical (DiPippo, 2016, p. 155), and sufficient quality is maintained throughout any/all turbine stages.

Figures 10, 11, and 12 on the following pages show single-, double-, and triple-flash cycles, optimized for representative geofluid production at the critical point, where the gross power output is approximately maximized, per Figure 2. The quantity m is introduced to account for the branching and mixing of geofluid flows, expressing the mass flow rate fraction at each state point.

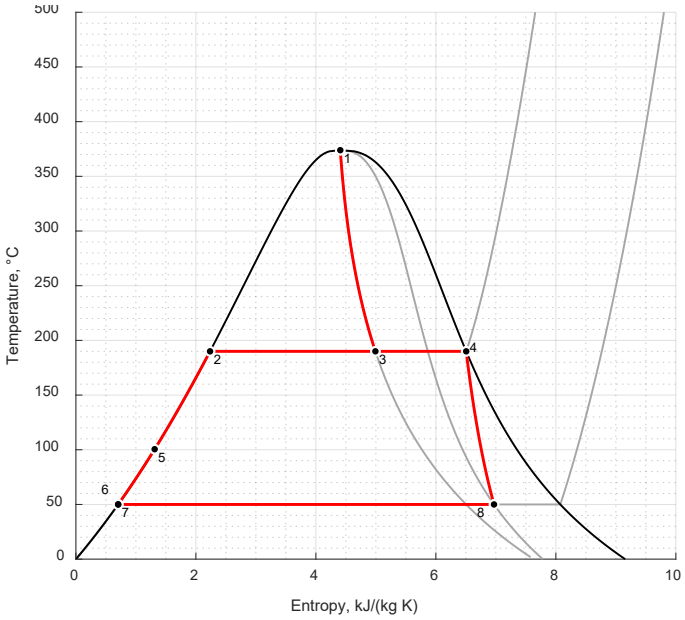

Direct-Use Single-Flash Cycle

q_in	1661.9	kJ/kg
q_out	1307.0	kJ/kg
w_net	354.9	kJ/kg
η_I	0.214	~
η_II	0.523	~
x_min	0.850	~

	T	P	h	s	x	m
1	373.9	220.64	2084.3	4.41	NaN	1.000
2	190.0	12.57	807.7	2.24	0.000	0.354
3	190.0	12.57	2084.3	4.99	0.646	1.000
4	190.0	12.57	2785.3	6.51	1.000	0.646
5	100.5	12.57	422.4	1.31	NaN	1.000
6	50.0	12.57	210.8	0.70	NaN	0.646
7	50.0	0.12	209.6	0.70	0.000	0.646
8	50.0	0.12	2234.2	6.97	0.850	0.646

Figure 10: Single-flash cycle for geofluid production at the critical point.

For a single-flash cycle, optimization generally entails maximizing the turbine inlet temperature, which is limited herein to about 190 °C according to the specifications of the turbine and condenser. Thereby, there is generally no dependence between the geofluid production conditions and the corresponding optimal flash cycle. The geofluid outlet temperature is typically high, at least 100 °C, indicating incomplete utilization of the geofluid.

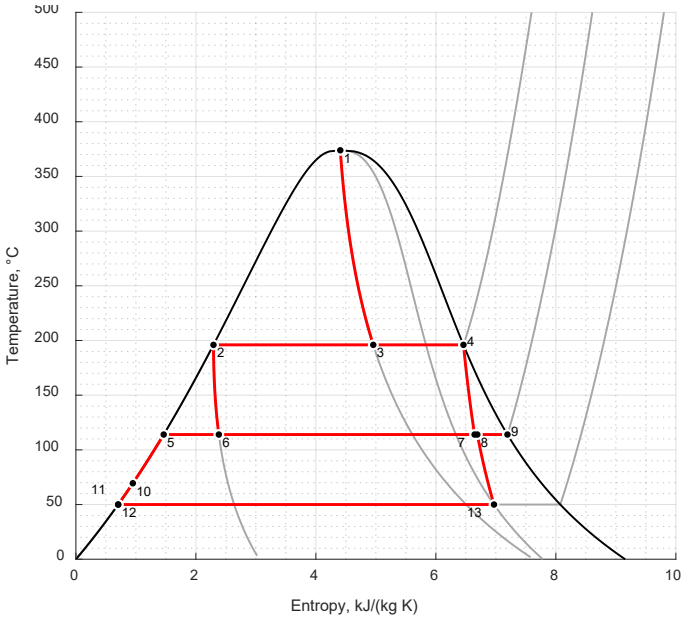

Direct-Use Double-Flash Cycle

q_in	1793.1	kJ/kg
q_out	1411.5	kJ/kg
w_net	381.7	kJ/kg
η_I	0.213	~
η_II	0.563	~
x_min	0.850	~

	T	P	h	s	x	m
1	373.9	220.64	2084.3	4.41	NaN	1.000
2	196.0	14.31	834.5	2.29	0.000	0.361
3	196.0	14.31	2084.3	4.96	0.639	1.000
4	196.0	14.31	2789.5	6.46	1.000	0.639
5	114.0	1.64	478.6	1.46	0.000	0.303
6	114.0	1.64	834.5	2.38	0.160	0.361
7	114.0	1.64	2485.0	6.65	0.904	0.639
8	114.0	1.64	2502.6	6.69	0.912	0.697
9	114.0	1.64	2697.2	7.19	1.000	0.058
10	69.5	1.64	291.1	0.95	NaN	1.000
11	50.0	1.64	209.7	0.70	NaN	0.697
12	50.0	0.12	209.6	0.70	0.000	0.697
13	50.0	0.12	2234.2	6.97	0.850	0.697

Figure 11: Double-flash cycle for geofluid production at the critical point.

Adding a second flash-separation process significantly reduces the geofluid outlet temperature, increasing the exergetic efficiency η_{II}. The small amount of vapor produced in the lower-pressure separator allows the temperature of the first separator to increase slightly, while maintaining the same turbine outlet conditions. The thermal efficiency η_I is essentially unchanged.

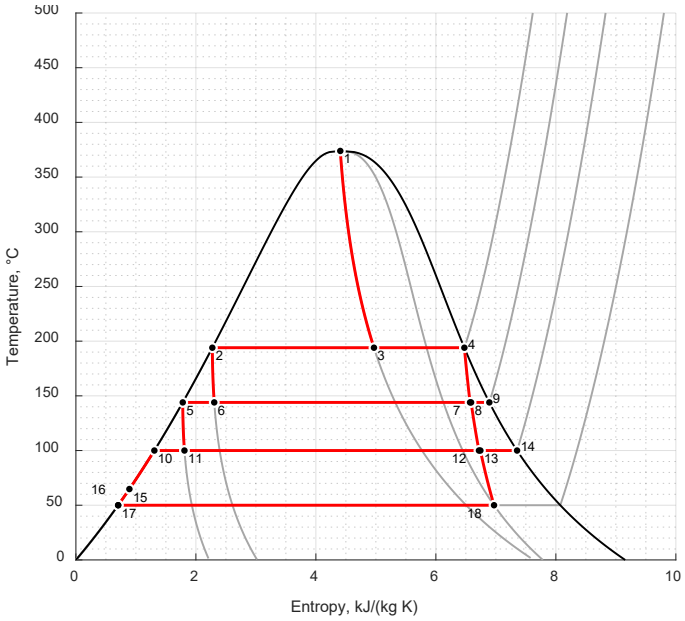

Direct-Use Triple-Flash Cycle

q_in	1812.7	kJ/kg
q_out	1427.3	kJ/kg
w_net	385.4	kJ/kg
η_I	0.213	~
η_II	0.568	~
x_min	0.850	~

	T	P	h	s	x	m
1	373.9	220.64	2084.3	4.41	NaN	1.000
2	194.0	13.71	825.5	2.27	0.000	0.359
3	194.0	13.71	2084.3	4.97	0.641	1.000
4	194.0	13.71	2788.2	6.47	1.000	0.641
5	144.0	4.05	606.6	1.78	0.000	0.322
6	144.0	4.05	825.5	2.31	0.103	0.359
7	144.0	4.05	2604.3	6.57	0.937	0.641
8	144.0	4.05	2611.6	6.59	0.940	0.678
9	144.0	4.05	2738.6	6.89	1.000	0.037
10	100.0	1.02	419.4	1.31	0.000	0.295
11	100.0	1.02	606.6	1.81	0.083	0.322
12	100.0	1.02	2438.4	6.72	0.895	0.678
13	100.0	1.02	2447.4	6.74	0.899	0.705
14	100.0	1.02	2675.6	7.35	1.000	0.027
15	64.8	1.02	271.5	0.89	NaN	1.000
16	50.0	1.02	209.6	0.70	NaN	0.705
17	50.0	0.12	209.6	0.70	0.000	0.705
18	50.0	0.12	2234.4	6.97	0.850	0.705

Figure 12: Triple-flash cycle for geofluid production at the critical point.

By contrast, adding a third flash-separation process yields less than a 1% improvement in η_{II}, and only about a 5 °C reduction in the geofluid outlet temperature. Likewise, there is no improvement in the thermal efficiency η_I. Unlike a more conventional flash cycle, e.g. at 150 °C, introducing a third flash does not significantly increase the vapor fraction at the turbine outlet, which is relatively high because of the large ΔT, ΔP, and Δx of the first flash alone.

Generally, the result of the gradient ascent optimization can be described as a variant of ETS, applied only between the first separator and the condenser, rather than between the inlet and the condenser, such that the first separator temperature is maximized, subject to the constraints of the turbine and condenser. This heuristic method yields a w_{net} that closely approximates the result via gradient ascent.

Figures 13, 14, and 15 on the following pages show the gross power outputs and exergetic efficiencies of single-, double-, and triple-flash plants, for geofluid produced in the subset of Region A where $h < 2{,}800$ kJ/kg.

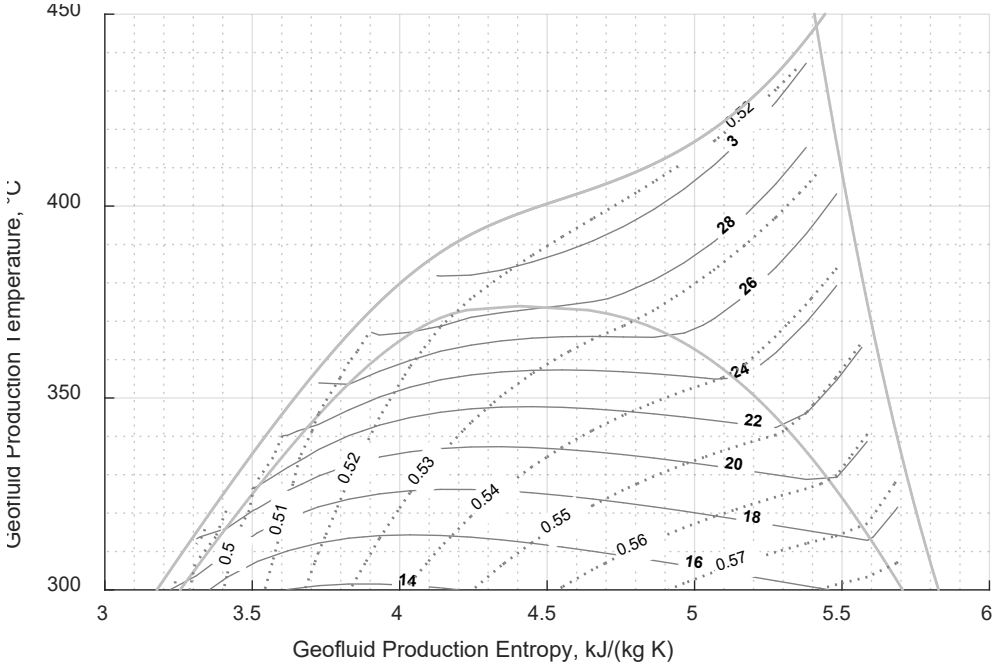

Figure 13: Gross power output in MWe (solid) and exergetic efficiency (dotted) for ideal single-flash cycles.

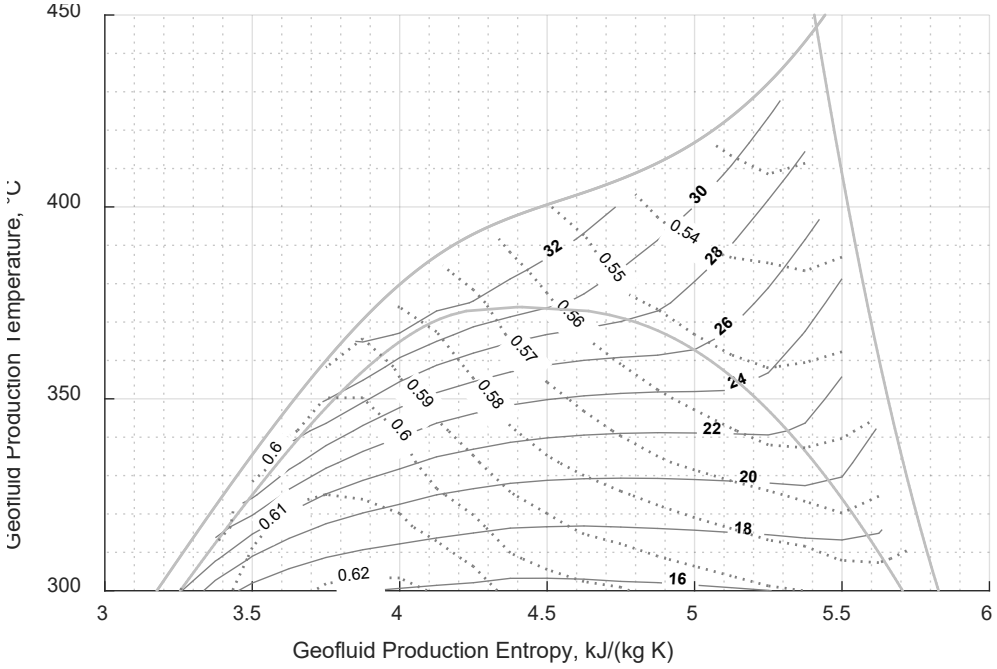

Figure 14: Gross power output in MWe (solid) and exergetic efficiency (dotted) for ideal double-flash cycles.

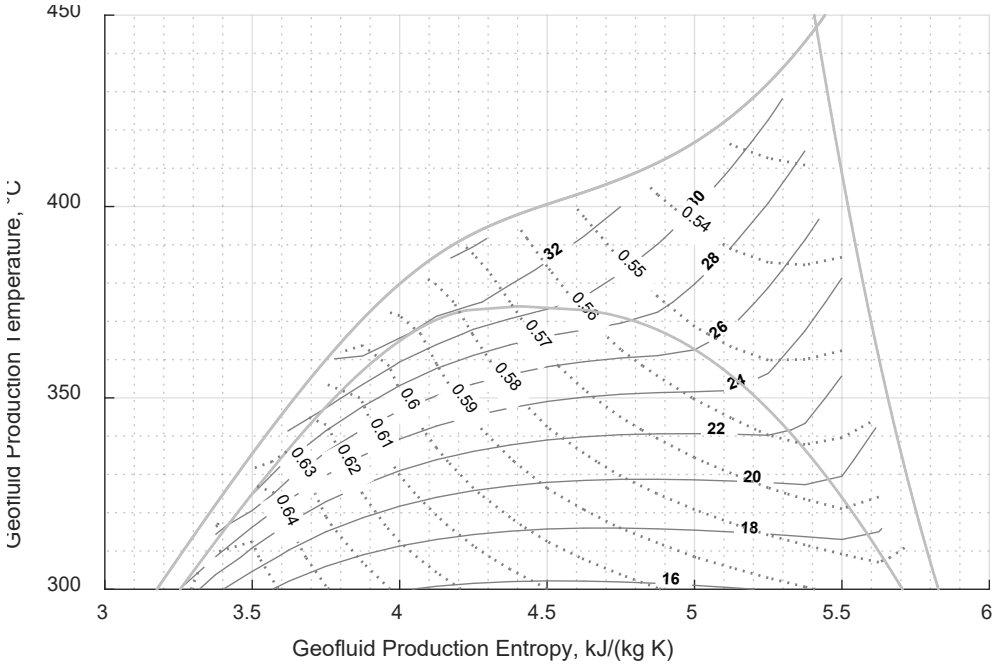

Figure 15: Gross power output in MWe (solid) and exergetic efficiency (dotted) for ideal triple-flash cycles.

These figures show ideal gross power outputs of up to about 30-32 MWe per well. In the subcritical region where $T < T_{crit}$, gross power output $\dot{Q}$ is generally maximized for a given temperature T in the compressed liquid region, confirming the earlier finding on the basis of exergetic power $\dot{E}$. Likewise, in the supercritical region where $T > T_{crit}$, gross power output $\dot{Q}$ increases with pressure P. In the subcritical region, as the quality of the produced geofluid x increases, there is less benefit to incorporating additional flashes, because the first flash alone yields a relatively high fraction of vapor m. The improvement to η_{II} associated with adding a second or third flash depends sensitively on the geofluid production conditions, with generally more improvement towards the liquid-dominated and supercritical regions. Notably, the maximum power attainable is approximately equal between the subcritical and the supercritical regions, indicating that attaining supercriticality is not necessary to maximize the gross power output. Further, the temperature required for maximum power output is significantly lower in the subcritical region.

The main drawbacks associated with flash cycles are their susceptibility to geofluid impurities, and their relatively large pump loads. The flash-separation process concentrates any solid impurities in the residual liquid of the flash vessel(s), which can cause scaling and fouling (DiPippo, 2016, p. 156), while permitting non-condensible gases (NCGs) such as carbon dioxide, methane, and hydrogen sulfide to enter the turbine and condenser, which reduces performance, increases corrosion, and can require specialized treatment (DiPippo, 2016, pp. 660-661). Particularly for subsurface systems requiring high-pressure reinjection, the large amount of geofluid pressure dissipated by the flash cycle increases the plant's parasitic pump load: for example, pressurizing 100 kg/s of water by 100 bar requires at least 1 MWe. Both drawbacks are mitigated by binary cycles, as described in the following section.

7. Binary Cycles

Whereas flash cycles use the produced geofluid directly, binary cycles instead transfer the geofluid's heat to a secondary working fluid in a series of counterflow heat exchangers, producing vapor suitable for a turbine. The main benefit of this approach is that the plant is less exposed to any contaminants that may be present in the produced geofluid, because the geofluid and working fluid do not mix (DiPippo, 2016, pp. 193-234). Because the heat transfer from the geofluid to the working fluid is ideally isobaric, the geofluid may require less pressurization before reinjection as compared to a flash plant, and thereby may incur less parasitic pump load. A schematic is shown in Figure 16 below.

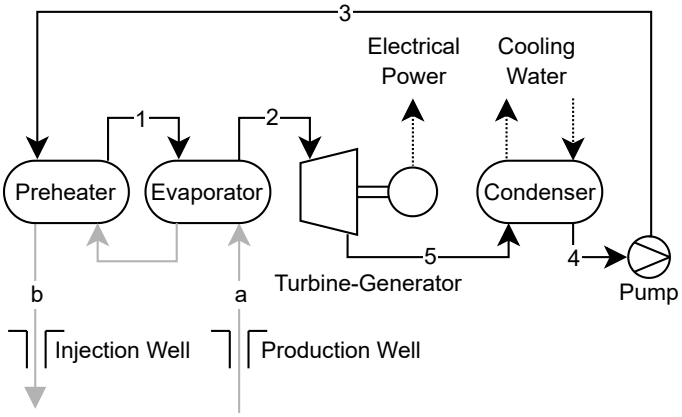

Figure 16: Schematic of a single-pressure binary plant, not to scale. Black arrows denote working fluid, and gray arrows denote geofluid.

The main irreversibility inherent to binary cycles is the heat transfer in the heat exchangers. Because heat can only transfer spontaneously in the direction of decreasing temperature, the working fluid can only approach, but cannot attain, the geofluid's production temperature. Thereby, vaporizing the working fluid inherently destroys some of the geofluid's initial exergy. This loss can be compared to the flash process of flash cycles, which is similarly irreversible and destructive of exergy.

This irreversibility can be mitigated in several ways, the most significant of which is the choice of working fluid. Ideally, the working fluid maintains a constant, small temperature difference ΔT at all points throughout the heat exchanger, as heat is transferred from the geofluid. The degree to which an actual heat transfer approaches this ideal "matched" condition is commonly evaluated using temperature-heat transfer, or T-q, diagrams.

Organic Rankine cycles, or ORCs, are a type of binary cycle that use a hydrocarbon working fluid, most commonly isobutane, butane, isopentane, or pentane, in order of increasing critical temperature. These are well-suited for typical geofluid production temperatures of 100-250 °C (Zarrouk and Moon, 2014, p. 150). This can be understood in terms of the match between the geofluid production temperature and the working fluid critical temperature, the latter of which ranges from 134.6-196.5 °C for the hydrocarbons cited. An additional benefit of an ORC is a relatively compact, dry turbine, because of the high density and retrograde condensation of hydrocarbon vapor, in both senses unlike steam.

However, it is not practical to superheat a hydrocarbon working fluid much beyond its critical temperature. This tends to increase q_{in} approximately as much as q_{out}, such that there is only marginal benefit to w_{net}, η_I, and η_{II}; that is, any superheat added before the turbine must be rejected in approximately equal magnitude by the condenser, as shown in Figure 17 below. This can be attributed to hydrocarbons' retrograde condensation, which causes superheating of the working fluid in the turbine, rather than partial condensation. Secondarily, fluid density decreases sharply after the critical point, progressively inhibiting heat transfer. For these reasons, ORCs do not typically exceed about 200 °C.

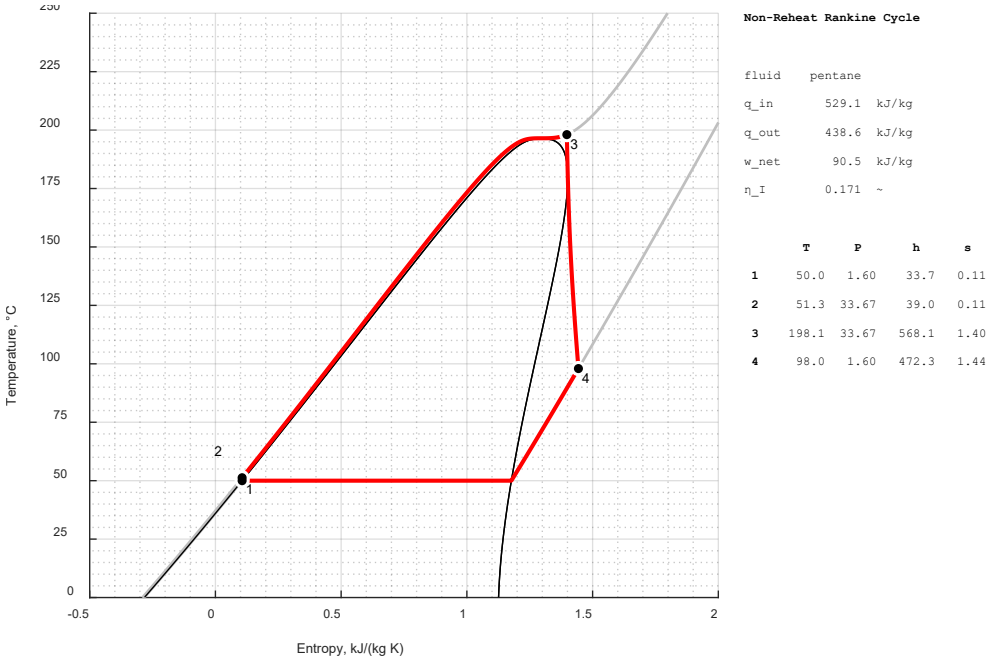

Figure 17: Supercritical pentane cycle, showing that any superheat added before the turbine, 3-4, must be rejected in approximately equal magnitude by the condenser, 4-1.

Because of this limitation, it can be shown using the methods developed later in this section that water outperforms typical ORC hydrocarbons for geofluid production temperatures exceeding about 315 °C, as shown in Figure 18 below. Note that each working fluid's critical temperature T_{crit} correlates to the range of geofluid production temperatures over which it is best suited. It can also be shown that cyclopentane ($T_{crit} = 238.5$ °C) has comparable performance to water over this temperature range, although no such plants are known to exist, and it compares unfavorably in cost, toxicity, and flammability. For these reasons, water is considered as the working fluid of choice for geofluid produced at 300-500 °C.

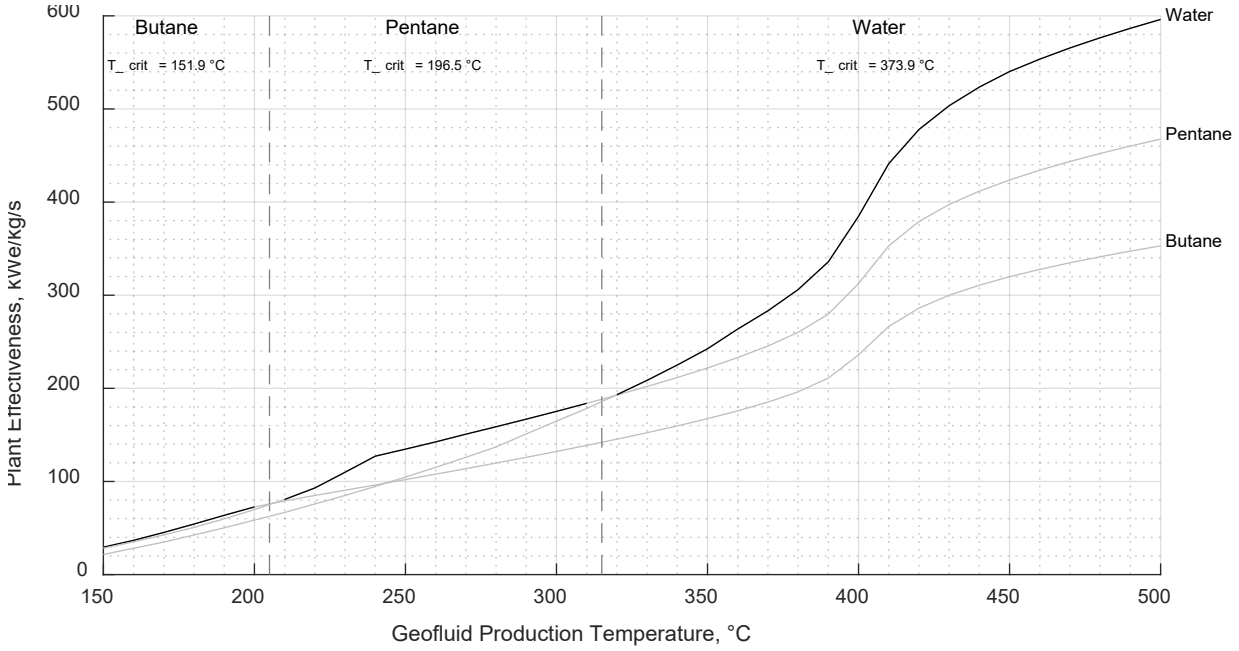

Figure 18: Optimized double-pressure binary plant effectiveness as a function of the working fluid composition and geofluid production temperature, for geofluid produced at 300 bar. Working fluids are emphasized in black over the temperature range for which they are best suited.

The simplest form of a binary cycle consists of two heat exchangers, or sets of heat exchangers, collectively called a preheater, and an evaporator. These produce saturated liquid, then saturated vapor, respectively, which is then supplied to a turbine. This configuration, sometimes referred to as single-pressure, typically has a single pinch point between the preheater and evaporator, where the temperature difference between the two fluids is minimized. The allowable value for this pinch point depends on hardware specifications, but is taken generically as $\Delta T_{pp} = 10$ °C herein. A dual- or double-pressure binary cycle improves on this design by adding an additional pump, preheater, and evaporator at a different pressure, producing vapor at two temperatures simultaneously that eventually mix in the turbine at the appropriate pressure. Typically, two pinch points occur, between both sets of preheaters and evaporators. Triple-pressure cycles are also possible, but are less common because of the diminishing returns associated with additional pressures.

Many of the same assumptions made earlier for ideal flash cycles also apply to ideal binary cycles, specifically: isobaric heat transfers, isentropic pumping, and mixing governed by conservation of mass and energy. Superheating is theoretically possible in binary cycles, but can be shown to confer only marginal benefit, and is less practical because of the decrease in heat transfer efficiency, so is not considered herein. The parameters governing the turbine(s) and condenser are taken as identical to the flash cycles described earlier.

For a given geofluid production scenario and working fluid selection, the remaining parameters required to define a cycle are the quantity of pressure(s), their associated saturation temperature(s), and for multi-pressure cycles specifically, the relative mass flow rate at each pressure. No flow branching occurs in single-pressure cycles, so trivially $m = 1$ throughout these cycles. In double-pressure cycles, m_{HP} implicitly defines m_{LP} by conservation of mass, and likewise with m_{HP}, m_{IP}, and m_{LP} in triple-pressure cycles, where HP, IP, and LP denote the high-, intermediate-, and low-pressure loops. The geofluid's T-q curve, and thereby the q_{out} or Δh of the geofluid, is determined by the bisection method, using the working fluid's T-q curve, and the specified ΔT_{pp}.

Optimization is either one-, three-, or five-dimensional, depending on the choice of a single-, double-, or triple-pressure cycle, respectively. The optimal values of these parameters are again determined using a gradient ascent algorithm, with fixed step sizes of 1 °C for T, and 0.01 (or 1%) for m. The optimization criterion is the exergetic efficiency η_{II} of the coupled geofluid-working fluid system, or equivalently its net work w_{net}. Local minima typically exist in η_{II} for double- and triple-flash cycles, such that converged solutions from the gradient ascent method are not necessarily global optima, but close approximations of it. Optimization is again constrained such that the evaporator(s) do not operate at sub-atmospheric pressure.

The mass flow rate of the working fluid is related to that of the geofluid by conservation of energy; that is, the heat power of the geofluid is ideally equal and opposite to that of the working fluid, neglecting leakage:

$$\dot{m}_g \, \Delta h_g = \dot{m}_w \, \Delta h_w \tag{14}$$

Where the subscripts g and w denote the geofluid and working fluid, respectively. Since $\Delta h_w = q_{in}$, the mass flow rate of the working fluid cycle can be expressed as:

$$\dot{m}_w = \frac{\dot{m}_g \, \Delta h_g}{q_{in}} \tag{15}$$

Figures 19, 20, and 21 on the following pages show T-s and T-q charts for single-, double-, and triple-pressure binary cycles, for representative geofluid production at the critical point.

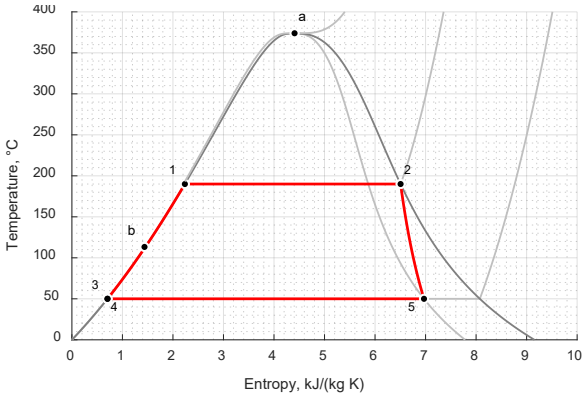

Single-Pressure Binary Cycle

q_in	2574.5	kJ/kg
q_out	2024.7	kJ/kg
w_net	549.8	kJ/kg
η_I	0.214	~
x_min	0.850	~

	T	P	h	s	x	m
1	190.0	12.57	807.7	2.24	0.000	1.000
2	190.0	12.57	2785.3	6.51	1.000	1.000
3	50.0	12.57	210.8	0.70	NaN	1.000
4	50.0	0.12	209.6	0.70	0.000	1.000
5	50.0	0.12	2234.2	6.97	0.850	1.000

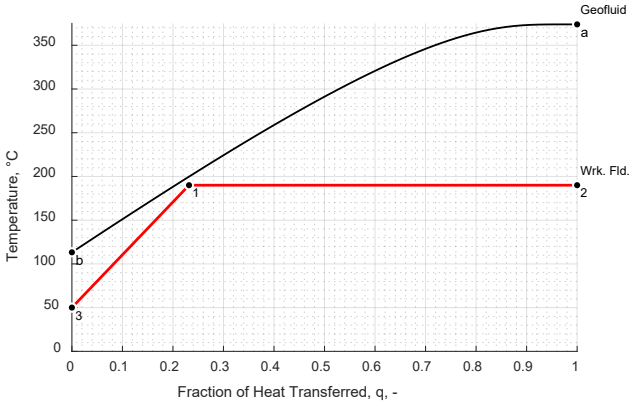

Geofluid

Nominal Pressure	220.6	bar
Inlet Temperature	373.9	°C
Inlet Enthalpy	2084.2	kJ/kg
Outlet Temperature	113.3	°C
Outlet Enthalpy	491.3	kJ/kg
Mass Flow Rate	80.1	kg/s

Plant

Mass Flow Rate (Wrk. Fld.)	49.6	kg/s
Heat Input	127.6	MWt
Condenser Rejection	100.4	MWt
Gross Output	27.3	MWe
Exergetic Efficiency, η_II	0.502	~

Figure 19: Single-pressure binary cycle for geofluid production at the critical point.

The optimal single-pressure working fluid cycle is generally independent of the geofluid production conditions. Maximizing η_{II} entails maximizing the turbine's inlet temperature, which is limited herein to about 190 °C per the constraints of the turbine and condenser. A single pinch point occurs between the preheater and evaporator, at State 1. The geofluid outlet temperature is generally high, at more than 100 °C, except where production is vapor-dominated; in these latter cases, the condensation of the geofluid in the evaporator with $\partial T/\partial q = 0$ increases the geofluid's $\partial T/\partial q$ in the preheater, improving the T-q curve match, and decreasing the geofluid outlet temperature.

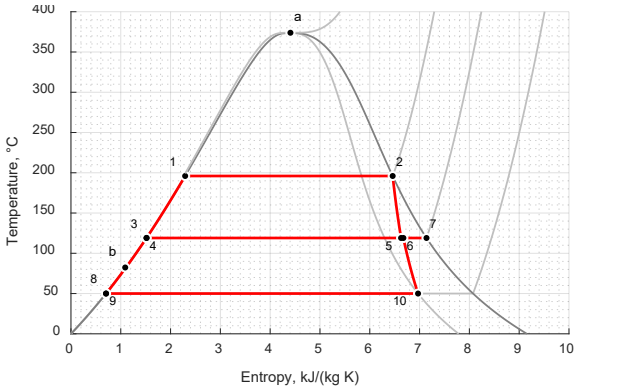

Double-Pressure Binary Cycle

q_in	2570.9	kJ/kg
q_out	2025.0	kJ/kg
w_net	546.0	kJ/kg
η_I	0.212	~
x_min	0.850	~

	T	P	h	s	x	m
1	196.0	14.31	834.5	2.29	0.000	0.910
2	196.0	14.31	2789.5	6.46	1.000	0.910
3	119.1	14.31	501.1	1.52	NaN	0.910
4	119.0	1.93	499.8	1.52	0.000	1.000
5	119.0	1.93	2504.4	6.63	0.909	0.910
6	119.0	1.93	2522.4	6.67	0.917	1.000
7	119.0	1.93	2704.5	7.14	1.000	0.090
8	50.0	1.93	209.7	0.70	NaN	1.000
9	50.0	0.12	209.6	0.70	0.000	1.000
10	50.0	0.12	2234.5	6.97	0.850	1.000

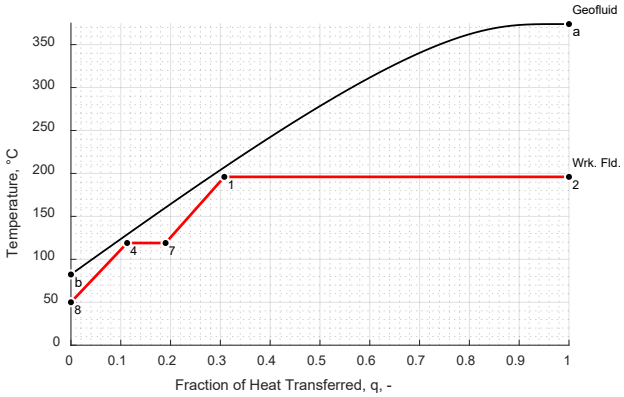

Geofluid

Nominal Pressure	220.6	bar
Inlet Temperature	373.9	°C
Inlet Enthalpy	2084.2	kJ/kg
Outlet Temperature	82.4	°C
Outlet Enthalpy	362.5	kJ/kg
Mass Flow Rate	80.1	kg/s

Plant

Mass Flow Rate (Wrk. Fld.)	53.7	kg/s
Heat Input	138.0	MWt
Condenser Rejection	108.7	MWt
Gross Output	29.3	MWe
Exergetic Efficiency, η_II	0.539	~

Figure 20: Double-pressure binary cycle for geofluid production at the critical point.

Adding a second vaporization pressure enables a better T-q curve match and a lower geofluid outlet temperature, conferring a significant improvement in exergetic efficiency η_{II}, and by extension gross power output $\dot{Q}$. Two pinch points occur between both pairs of preheaters (8-4, 3-1) and evaporators (4-7, 1-2). Optimization equalizes the magnitudes of these two pinch points at States 1 and 4. Most of the working fluid flows through the HP loop, with the small remainder flowing through the LP loop, enabling a slightly higher turbine inlet temperature. The thermal efficiency η_I is essentially unchanged.

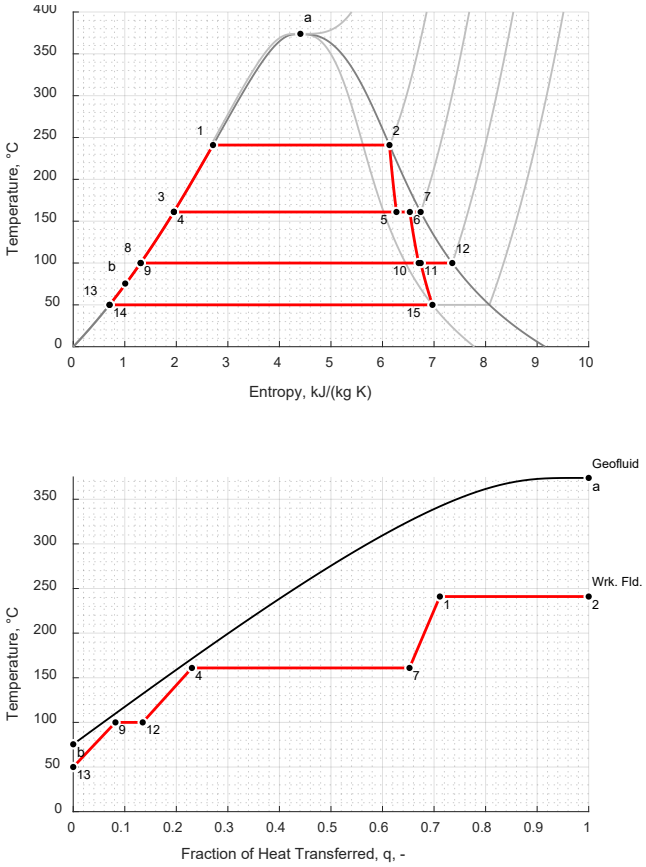

Triple-Pressure Binary Cycle

fluid	water
q_in	2560.8 kJ/kg
q_out	2024.6 kJ/kg
w_net	536.1 kJ/kg
η_I	0.209 ~
x_min	0.850 ~

	T	P	h	s	x	m
1	241.0	34.09	1042.6	2.71	0.000	0.420
2	241.0	34.09	2802.8	6.13	1.000	0.420
3	161.3	34.09	683.1	1.95	NaN	0.420
4	161.0	6.35	680.0	1.95	0.000	0.940
5	161.0	6.35	2554.7	6.27	0.902	0.420
6	161.0	6.35	2667.5	6.53	0.956	0.940
7	161.0	6.35	2758.6	6.74	1.000	0.520
8	100.0	6.35	419.9	1.31	NaN	0.940
9	100.0	1.02	419.4	1.31	0.000	1.000
10	100.0	1.02	2432.5	6.70	0.892	0.940
11	100.0	1.02	2447.1	6.74	0.899	1.000
12	100.0	1.02	2675.6	7.35	1.000	0.060
13	50.0	1.02	209.6	0.70	NaN	1.000
14	50.0	0.12	209.6	0.70	0.000	1.000
15	50.0	0.12	2234.2	6.97	0.850	1.000

Geofluid

Nominal Pressure	220.6	bar
Inlet Temperature	373.9	°C
Inlet Enthalpy	2084.2	kJ/kg
Outlet Temperature	75.5	°C
Outlet Enthalpy	334.0	kJ/kg
Mass Flow Rate	80.1	kg/s

Plant

Mass Flow Rate (Wrk. Fld.)	54.8	kg/s
Heat Input	140.3	MWt
Condenser Rejection	110.9	MWt
Gross Output	29.4	MWe
Exergetic Efficiency, η_II	0.540	~

Figure 21: Triple-pressure binary cycle for geofluid production at the critical point.

By contrast, adding a third vaporization pressure does not confer significant benefit to thermal efficiency η_I or exergetic efficiency η_{II}, and thereby does not appear to be economical. This can be seen heuristically from the optimized T-q curves, which show only two significant pinch points at States 4 and 9, one less than the maximum implied by the quantity of vaporization pressures.

Figures 22, 23, and 24 on the following pages show the gross power outputs and exergetic efficiencies of single-, double-, and triple-pressure binary plants for geofluid produced in Region A.

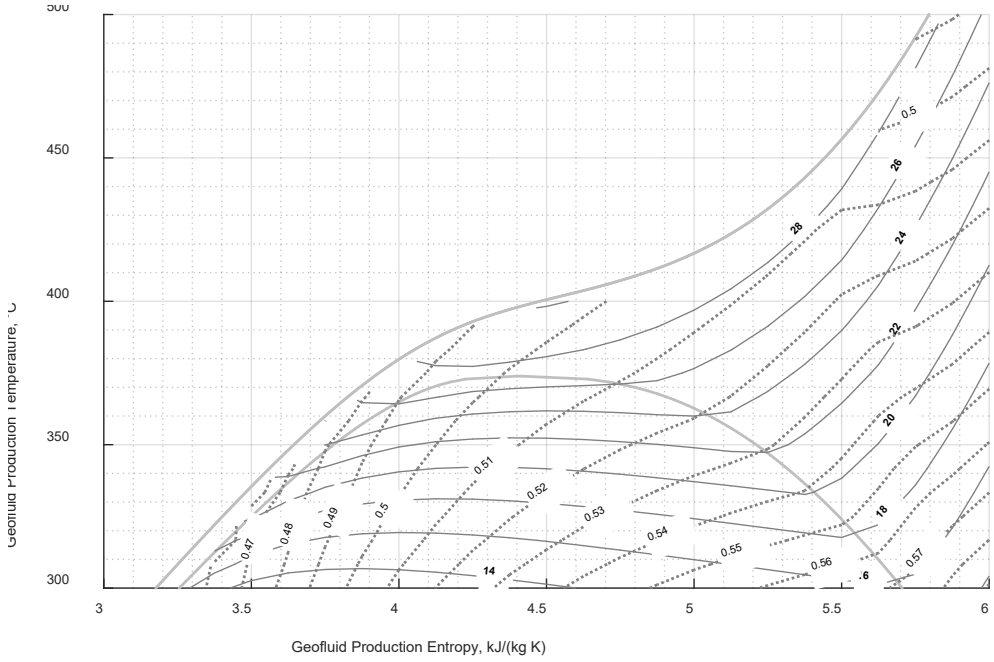

Figure 22: Gross power output in MWe (solid) and exergetic efficiency (dotted) for ideal single-pressure binary cycles.

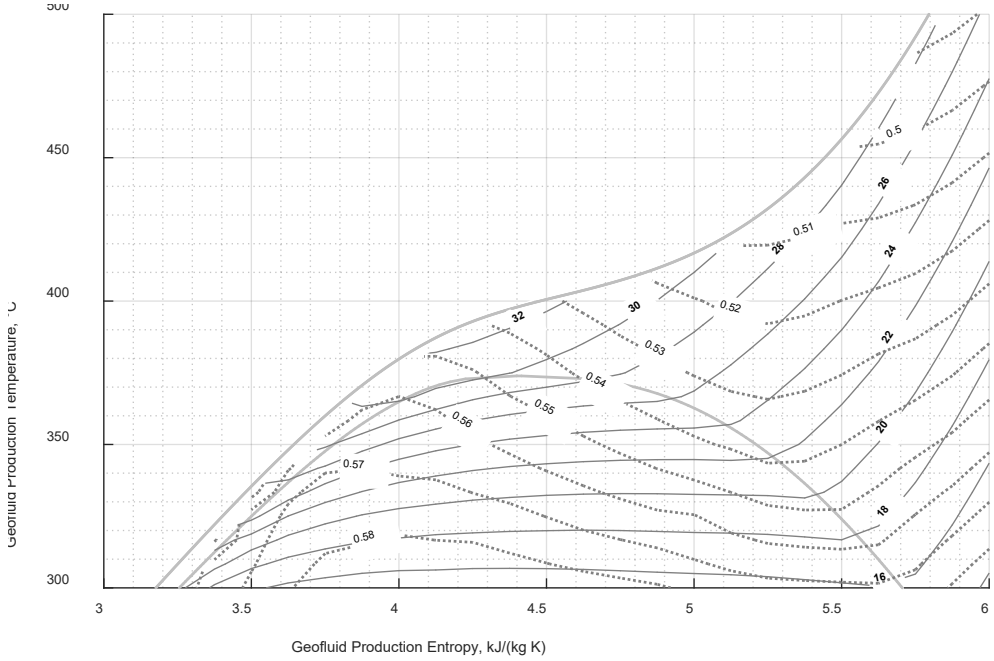

Figure 23: Gross power output in MWe (solid) and exergetic efficiency (dotted) for ideal double-pressure binary cycles.

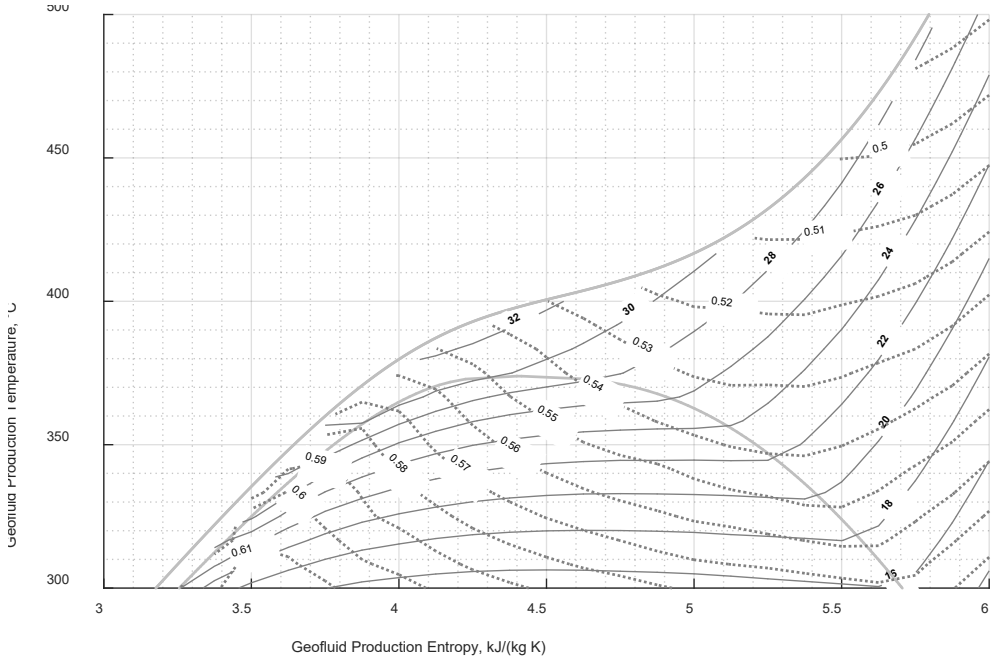

Figure 24: Gross power output in MWe (solid) and exergetic efficiency (dotted) for ideal triple-pressure binary cycles.

These plots show that the characteristics of ideal high-temperature binary plants are highly comparable to those of high-temperature flash plants. The gross power output is increased significantly by introducing a second vaporization pressure, while introducing a third vaporization pressure confers benefit mainly towards the liquid-dominated region. For a given temperature T, the gross power output $\dot{Q}$ is generally maximized where the geofluid production is densest, corresponding to the phase regions of compressed liquid and supercritical fluid. The gross power output increases significantly with temperature in the subcritical region, and less significantly with pressure in the supercritical region.

8. Conclusion

This paper considered the ideal gross output of a generic geothermal power system producing between 300-500 °C. The characteristically high slenderness of the production well imposes significant hydraulic constraints on geofluid production. Accordingly, the maximum mass flow rate of a production well with an 8.5" minimum inner diameter was found to be about 100 kg/s. Combining this hydraulic constraint with the thermodynamic constraint associated with exergy indicated that exergetic power is maximized in the compressed liquid and supercritical regions of water, at about 55-60 MWe, which have characteristic production pressures of $P > 85.9$ bar in the subcritical region, and $P > 220.6$ bar in the supercritical region. Further, it was noted that exergetic power plateaus around the critical point of water, after which gains in exergy are approximately offset by losses in mass flow rate, suggesting that supercriticality is not necessary for maximum performance.

Geofluid production was classified into two regions, A and B, based on suitability for supplying typical non-reheat steam turbines. Region B was defined as being sufficient for a dry steam power cycle, while Region A required a more complex power cycle, i.e. flash or binary, to attain sufficient turbine dryness.

Dry steam power cycles in Region B were found to be superior in terms of exergetic efficiency, ideally around 78-84%, because no processing of the geofluid is required, entailing minimal irreversibility. However, the gross power output is limited by the characteristically low geofluid production density, limiting the production mass flow rate and pressure.

Flash cycles were considered in the subset of Region A where $h < 2{,}800$ kJ/kg, i.e. where isenthalpic expansion generally produces a two-phase mixture. The conventional "equal-temperature-split" (ETS) guideline for flash separator temperatures was shown to break down above about 200 °C, as the temperature approaches the critical point where the specific heat becomes undefined. Instead, a gradient ascent algorithm was used to determine the optimal separator temperatures that maximize the cycle's exergetic efficiency. Single-, double-, and triple-flash cycles were evaluated, showing substantially greater gross power output on an equal-temperature basis, as compared to the earlier dry steam power cycles. Though the exergetic efficiency was lower, at 50-65%, this was more than compensated for by the denser geofluid production, yielding higher mass flow rates. It was noted as a heuristic approximation that ETS applied between the first separator at the highest possible temperature and the condenser yielded a net work that closely matched the result obtained via gradient ascent. Adding a second or third flash was found to be more effective towards the liquid-dominated and supercritical regions. Drawbacks associated with solid and gaseous geofluid impurities, as well as pump loads, were noted.

Binary cycles were also considered in Region A. The choice of working fluid was considered as the primary means of mitigating the irreversibility inherent to this type of cycle. It was shown that the hydrocarbon working fluids characteristic of organic Rankine cycles (ORCs) cannot practically attain temperatures exceeding about 200 °C because of their retrograde condensation. As a result, water was found to outperform these hydrocarbons above a geofluid production temperature of about 315 °C, and was considered as the working fluid of choice. A gradient ascent algorithm was again used to determine the optimal evaporator temperature(s) and mass flow rate fraction(s) to maximize the cycle's exergetic efficiency, accounting for pinch points between the two fluids in T-q coordinates. The thermal efficiencies, exergetic efficiencies, and gross power outputs of these optimized cycles, in single-, double-, and triple-pressure variations, were found to be highly comparable to flash cycles of equal sophistication. This can be attributed to the many properties that are shared between the two cycles, including the working fluid composition, the turbine performance, and the heat rejection scheme. In this sense, binary plants attain performance comparable to flash plants, with significantly less susceptibility to geofluid impurities, and potentially with less parasitic pumping load.

As a whole, this work indicates that geothermal systems may attain their maximum power output with a production temperature as low as 350-375 °C, i.e. near the critical temperature, provided that the production pressure is sufficiently high. For a production well with an 8.5” minimum inner diameter, the ideal power output is about 30-32 MWe gross, using either a double-flash cycle, or a double-pressure binary cycle. This represents the potential of up to an order of magnitude improvement over the typical performance of current geothermal systems.

Nomenclature

The symbols shown in Table 1 below are used throughout this paper. Where applicable, the assumed value is also shown.

Symbol	Definition	Value	Units
C_p	Specific heat capacity, isobaric	-	J/(kg K)
$\dot{E}$	Exergetic power	-	MW, or MWe
$\dot{Q}$	Gross power output	-	MWe
T_{cond}	Condenser temperature	50	°C
T_{crit}	Critical temperature	-	°C
T_o	Temperature, dead state	50	°C
$\dot{m}$	Mass flow rate	-	kg/s
q_{in}	Heat input	-	kJ/kg
q_{out}	Heat output, or rejection	-	kJ/kg
v_e	Erosional velocity	-	m/s
w_{net}	Net work	-	kJ/kg
x_{min}	Turbine minimum quality	0.85	-
η_I	Thermal (First Law) efficiency	-	-
η_{II}	Exergetic (Second Law) efficiency	-	-
η_{td}	Turbine efficiency, dry, isentropic	0.85	-
h	Enthalpy	-	kJ/kg
Δ	Difference, or change	-	-
ΔT_{pp}	Temperature difference at pinch point	10	°C
A	Wellbore minimum cross-sectional flow area	0.0366	m^2
D	Wellbore minimum inner diameter	8.5	in
L	Wellbore length	-	m
P	Pressure	-	bar
T	Temperature	-	°C
c	Erosional constant, empirical, API RP 14E	100	$(ft/s)(lb/ft^3)^{1/2}$
e	Exergy	-	kJ/kg
f	Friction factor	-	-
m	Mass flow rate fraction	-	-
q	Fraction of heat transferred	-	-
s	Entropy	-	kJ/(kg K)
v	Velocity	-	m/s
x	Quality, or dryness fraction	-	-
δ	Partial derivative	-	-
ρ	Density	-	kg/m^3

Table 1: List of symbols used in this paper, and assumed values, where applicable.

REFERENCES

American Petroleum Institute. "API RP 14E: Recommended Practice for Design and Installation of Offshore Production Platform Piping Systems." 5th ed. (1991, reaffirmed 2013).

American Petroleum Institute. "API Specification 5CT: Specification for Casing and Tubing." 8th ed. (2005).

Calpine Corporation. "The Geysers Geothermal Field 2022 Statistics." Mar. 2023, https://geysers.com/The-Geysers/Geysers-By-The-Numbers.

Çengel, Y., et al. "Fundamentals of Thermal-Fluid Sciences". McGraw-Hill (2012).

DiPippo, R. "Geothermal Power Plants: Principles, Applications, Case Studies and Environmental Impact". Elsevier/Butterworth-Heinemann (2016).

Ingason, K., et al. "Design and Development of the Discharge System of IDDP-1." *Geothermics* (2014).

International Finance Corporation (IFC), and GeothermEx, Inc. "Success of Geothermal Wells: A Global Study." (2013).

Lemmon, E. W., et al. "NIST Standard Reference Database 23: Reference Fluid Thermodynamic and Transport Properties-REFPROP, Version 10.0, National Institute of Standards and Technology." (2018).

Zarrouk, S., and Moon, H. "Efficiency of Geothermal Power Plants: A Worldwide Review." *Geothermics* (2014).